ISSN 1070-3284, Russian Journal of Coordination Chemistry, 2013, Vol. 39, No. 7, pp. 519–523. © Pleiades Publishing, Ltd., 2013.

A Novel 2D Phosphomolybdate Hybrid $[Cu(En)(EnH)]_2[P_2Mo_5O_{23}] \cdot 3H_2O$ Constructed from Strandberg-Type Polyoxometalate Units and Copper-Organic Cation Bridges[1]

J. W. Zhao[a, *], Y. Y. Li[a], Y. H. Wang[b], D. Y. Shi[a], J. Luo[a], and L. J. Chen[a, *]

[a] *Institute of Molecular and Crystal Engineering, College of Chemistry and Chemical Engineering, Henan University, Kaifeng, Henan, 475004 P.R. China*

[b] *Zhejiang Huate New Material Co., Ltd., Hangzhou, Zhejiang, 311300 P.R. China*

**e-mail: zhaojunwei@henu.edu.cn, ljchen@henu.edu.cn*

Received November 15, 2011

Abstract—A 2D Strandberg-type phosphomolybdate hybrid $[Cu(En)(EnH)]_2[P_2Mo_5O_{23}] \cdot 3H_2O$ (**I**) (En = ethylenediamine) has been successfully synthesized under hydrothermal conditions and structurally characterized by elemental analyses, IR spectrum, UV spectrum and single-crystal X-ray diffraction. The molecular structural unit of **I** consists of one Strandberg-type $[P_2Mo_5O_{23}]^{6-}$ subunit, two $[Cu(En)(EnH)]^{3+}$ cations and three lattice water molecules. The most remarkable feature of **I** is that each molecular structural unit is connected with adjacent four same units by four $[Cu(En)(EnH)]^{3+}$ bridges constructing the 2D organic-inorganic hybrid sheet structure with a 4-connected topology. As far as we know, such 2D hybrid sheet structure constructed from Strandberg-type phosphomolybdate units and copper-organic cation bridges is very rare.

DOI: 10.1134/S1070328413060122

INTRODUCTION

Polyoxometalates (POMs) are attractive anionic metal-oxygen clusters with definite size and shape and have attracted great attention in recent years because of a variety of structures and properties and a multitude of potential applications in catalysis, materials science, and medicine [1–3]. Among them, phosphomolybdates with the Mo : P ratio varing from 2.5 to 12 have developed as a particularly well-researched subfamily [4], of which the Strandberg-type diphosphopentamolybdate (DPPM) clusters with the general formula of $[H_xMo_5P_2O_{23}]^{(6-x)-}$ ($x = 0$, 1, 2) as a very important subfamily have attracted considerable interest due to their unexpected architectures, special characteristics or even new synergetic functional properties in the complementary design of solid-state structures with different composites [5, 6], since the structure of the first Strandberg-type DPPM $Na_6[P_2Mo_5O_{23}] \cdot 13H_2O$ was determined in [7]. Later, the structures of $Na_4[H_2P_2Mo_5O_{23}] \cdot 10H_2O$ and $(NH_4)_5[HP_2Mo_5O_{23}] \cdot 3H_2O$ were successively determined [8, 9]. Four organoammonium DPPMs $(C_5H_7N_2)_6[P_2Mo_5O_{23}] \cdot 5H_2O$, $(C_2H_{10}N_2)_3[P_2Mo_5O_{23}] \cdot 6H_2O$, $Al(C_4H_{15}N_3)_4[HP_2Mo_5O_{23}]_2Cl \cdot 10H_2O$, and $(C_4H_{12}N)_4[H_2P_2Mo_5O_{23}] \cdot 5H_2O$ were prepared in [10]. Hong's group communicated a nucleobase–inorganic hybrid polymer $[CuP_2Mo_5O_{23}(H_2O)_2(Hcyt)_4]_n$ built from $P_2Mo_5O_{23}$ and Cu(II)-cytosine subunits [11]. An organic-inorganic compsite DPPM $(C_6H_{11}NH_3)_5H(P_2Mo_5O_{23}) \cdot 4H_2O$ was reported in [12]. Upreti and Ramanan studied the role of hydrogen-bonded interactions in the crystal packing of phenylenediammonium DPPM solids $\{NH_3C_6H_4NH_3\}_7[Mo_5O_{15}\{PO_3(OH)\}_2]_2[HMo_5O_{15}\{PO_3(OH)\}_2]_2 \cdot 21H_2O$, $\{NH_3C_6H_4NH_3\}_2[Mo_5O_{15}\{PO_3(OH)\}_2] \cdot 4H_2O$, and $\{NH_3C_6H_4NH_3\}_2\{NH_2C_6H_4NH_3\}[Mo_5O_{15}\{PO_4\}\{PO_3(OH)\}] \cdot 3H_2O$ [13]. As shown above, organic components are in the form of protonation and often function as the charge compensation cations in the most reported DPPMs. Therefore, exploring and constructing the extended structures built by Strandberg-based DPPM units by employing the metal coordination complexes as linkers to integrate have become one of the most challenging topics in POM synthetic chemistry. A 1D chain-like DPPM $[Cu(2,2'\text{-Bipy})(H_2O)_2]_5[Cu(2,2'\text{-Bipy})(H_2O)]\}[P_2Mo_5O_{23}]_2 \cdot 10H_2O$ was isolated in [6]. In the participation of copper-pyrazole complex templating agent, a class of DPPM hybrids with 1D, 2D, and 3D architectures were obtained from an aqueoussolution containing sodium molybdate, cupric chloride and pyrazole acidified with phosphoric acid [14]. A 1D DPPM hybrid $Mg[Cu(Bim)(H_2O)]_2[P_2Mo_5O_{23}] \cdot 4H_2O$ was addressed by Zhou' group [5]. We have initiated research on the P–Mo–O system. A novel type of heteropolyoxoanion precursor $\{[Ca(H_2O)]_6[P_4Mo_6O_{34}]_2\}^{12-}$ was firstly discovered in [15]. As a part of our continuour work, we have obtained a novel 2D Strandberg-type

[1] The article is published in the original.

Crystallographic data and structural refinements for **I**

Parameter	Value
Formula weight	1333.20
Crystal system	Orthorhombic
Space group	*Ibca*
a, Å	11.533(5)
b, Å	15.321(7)
c, Å	39.235(17)
V, Å^3	6933(5)
Z	8
ρ_{calcd}, g cm^{-3}	2.555
μ, mm^{-1}	3.150
$F(000)$	5200
Crystal size, mm	0.20 × 0.14 × 0.08
Limiting indices	$-12 \le h \le 13$, $-18 \le k \le 17$, $-27 \le l \le 46$
θ Range for data collection, deg	2.44–25.00
Type of scan	φ and ω scan
Number of reflections, $I > 2\sigma(I)$	2850
Reflections collected/unique (R_{int})	16161/3003 (0.0233)
Number of parameters refined	233
Goodness-of-fit on F^2	1.075
Final R indices ($I > 2\sigma(I)$)	$R_1 = 0.0236$, $wR_2 = 0.0626$
R indices (all data)	$R_1 = 0.0250$, $wR_2 = 0.0632$
$\Delta\rho_{max}/\Delta\rho_{min}$, e Å^{-3}	1.704/−0.759

phosphomolybdate hybrid $[Cu(En)(EnH)]_2[P_2Mo_5O_{23}] \cdot 3H_2O$ (**I**) by means of the POM precursor α-$Na_2HPMo_{12}O_{40} \cdot 14H_2O$, in which each molecular structural unit is combined with adjacent four same units by four $[Cu(En)(EnH)]^{3+}$ bridges creating the 2D organic-inorganic hybrid sheet structure. To the best of our knowledge, such 2D hybrid sheet structure constructed from Strandberg-type phosphomolybdate units and copper-organic cation bridges is very rare albeit two 2D Strandberg-type phosphomolybdates $\{Cu(Pz)_2(H_2O)_4\}[\{Cu(Pz)_2(H_2O)\}_2\{Cu(Pz)_4\}_2\{HP_2Mo_5O_{23}\}_2] \cdot 6H_2O$ and $[\{Cu(Pz)_2\}P_2Mo_2O_{12}(H_2O)_2]$ have been found [14].

EXPERIMENTAL

Materials and methods. α-$Na_2HPMo_{12}O_{40} \cdot 14H_2O$ was prepared according to the literature [16] and confirmed by IR spectrum. All other chemicals used for synthesis were reagent grade and used without further purification. Elemental analyses (C, H, and N) were performed on a PerkinElmer 240C elemental analyzer. The IR spectrum was recorded from a sample powder palletized with KBr on a Nicolet 170 SXFT-IR spectrometer in the range of 4000–400 cm^{-1}. The UV absorption spectrum was obtained with a U-4100 spectrometer at room temperature.

Synthesis of I. α-$Na_2HPMo_{12}O_{40} \cdot 14H_2O$ (0.306 g, 0.144 mmol), $CuCl_2 \cdot 2H_2O$ (0.033 g, 0.194 mmol), and $PrCl_3$ (0.033 g, 0.133 mmol) were suspended in H_2O (5 mL), to which En (0.100 mL, 1.480 mmol) and glacial acetic acid (0.05 mL, 0.874 mmol) were added under stirring. The resulting mixture was stirred for 3 h, sealed in a 25 mL Teflon-lined stainless steel autoclave, kept for 6 days at 160°C and then cooled to room temperature. Purple block crystals were filtered, washed with distilled water and dried in air at ambient temperature. The yield was ~31% (based on α-$Na_2HPMo_{12}O_{40} \cdot 14H_2O$).

For $C_8H_{40}N_8O_{26}P_2Cu_2Mo_5$			
anal. calcd., %:	C, 7.21;	H, 3.02;	N, 8.41.
Found, %:	C, 7.12;	H, 3.14;	N, 8.58.

Unfortunately, though $PrCl_3$ was used as the starting materials in the reaction, there was no Pr(III) in **I**. When $PrCl_3$ was removed away from the reactants, **I** was not formed. This result suggests that $PrCl_3$ plays a synergistic action with other components in the formation of **I** albeit the specific role was not well understood in the reaction. Similar phenomena have been previously encountered [17, 18]. For instance, during the course of synthesizing the $[EnH_2]_4\{[Cu(En)_2][(A\text{-}\beta\text{-}H_2AsW_9O_{34})Cu(En)_2]_2\} \cdot 8H_2O$, $ErCl_3$ was also used in the reaction system, however, no Er^{3+} ion was observed in the product phase [17]. Interestingly, the transformation of the Keggin-type $[\alpha\text{-}PMo_{12}O_{40}]^{3-}$ to the Strandberg-type $[P_2Mo_5O_{23}]^{6-}$ occurred, which was firstly oberved in POM chemistry.

X-ray crystal determination. Intensity data of **I** were collected on a Bruker APEX-II CCD detector at 296(2) K with a MoK_α radiation ($\lambda = 0.71073$ Å). The structure was solved by the direct method and refined by the full-matrix least-squares method on F^2 using the SHELXTL crystallographic software package [19]. Empirical absorption correction and Lorentz polarization correction were applied to the intensity data. Anisotropic thermal parameters were used to refine all non-hydrogen atoms. No attempt was made to locate the hydrogen atoms of water molecules. Hydrogen atoms on the En ligands were placed on calculated positions and included in the refinement riding on their respective parent atoms. The hydrogen atoms attached to lattice water molecules were not located. The weighting detail: $w = 1/[\sigma^2(F_o^2) + (0.0330P)^2 + 30.4037P]$, where $P = (F_o^2 + 2F_c^2)/3$. Details of the crystal data and final structure refinements of the compound are summarized in table. The atomic coordinates and other parameters of structure **I** have been deposited with the Cambridge Crystallographic Data Centre (no. 853748;

deposit@ccdc.cam.ac.uk or http://www.ccdc.cam.ac.uk).

RESULTS AND DISCUSSION

X-ray single-crystal diffraction indicates that the molecular structural unit of **I** is composed of a Strandberg-type $[P_2Mo_5O_{23}]^{6-}$ subunit, two $[Cu(En)(EnH)]^{3+}$ cations, and three lattice water molecules (Fig. 1a). The oxidation states of Cu, P, and Mo atoms are +2, +5, and +6, respectively, which are determinded by the bond valence sum (BVS) calculations (the BVS values of the Cu(1), P(1), Mo(1), Mo(2), and Mo(3) atoms are 1.98, 4.88, 5.88, 5.90, and 5.92, respectively) [20, 21]. Considering the charge balance of the molecular structural unit of **I**, two protons should be added. To locate the possible positions of two protons, BVS calculations of all the oxygen atoms on the $[P_2Mo_5O_{23}]^{6-}$ subunit have been performed (the BVS values: 1.62 for O(1), 1.67 for O(2), 1.98 for O(3), 1.87 for O(4), 1.80 for O(5), 1.77 for O(6), 1.69 for O(7), 1.90 for O(8), 1.68 for O(9), 1.82 for O(1)0, 1.64 for O(1)1, and 1.76 for O(11) [20, 21]. As shown above, the BVS values of all the oxygen atoms approach to 2, indicating that all the oxygen atoms are not protonated. As a result, the monodentate coordinating En molecule on $[Cu(En)(EnH)]^{3+}$ cation should be monoprotonated. In fact, the phenomena that N-containing organic molecules are often protonated under either acidic or basic conditions are very common in POM chemistry and coordination chemistry [22–25]. For example, a microporous Dawson-based POM solid $[H_3N(CH_2)_6NH_3]_4[W_{18}P_2O_{62}] \cdot 3H_2O$ with prontonated 1,6-diaminohexane molecules under acidic conditions was reported in [22]. Two phosphotungstates $K_4(C_2N_2H_{10})_{12}[(\alpha\text{-}PW_{10}Fe_2O_{39})_4] \cdot 30H_2O$ and $(C_2N_2H_{10})_{11}[\{(B\text{-}\alpha\text{-}PW_9O_{34})Fe_3(OH)_3\}_4(PO_4)_4Fe] \cdot 38H_2O$ were given in [23, 24], respectively, where En molecules are also protonated under weak basic conditions. As a result, the formula of **I** can be written as $[Cu(En)(EnH)]_2[P_2Mo_5O_{23}] \cdot 3H_2O$.

Since the evident Jahn–Teller distortion of Cu^{2+} cations in the crystal field often leads to the elongation of the Cu–O distances [17, 26, 27], the weak Cu–O interactions will be considered in the description of crystal structure of **I**. The Strandberg-type $[P_2Mo_5O_{23}]^{6-}$ subunit contains five MoO_6 octahedra, which form a pentagonal ring by sharing edges and corners, and two PO_4 tetrahedra connected to each side of the ring and sharing three oxygen atoms with different MoO_6 octahedra (Fig. 1b). The bond lengths of P–O range from 1.524(2) to 1.562(2) Å and Mo–O vary from 1.715(3) to 2.405(3) Å, respectively. All bond lengths and bond angles are within the normal ranges [7–14, 28]. Each MoO_6 octahedron has four bridging oxygen atoms and two terminal oxygen atoms. There are two types of Mo–Mo distances: (a) those between octahedra sharing edges (3.376–3.397 Å); (b) between octahedra

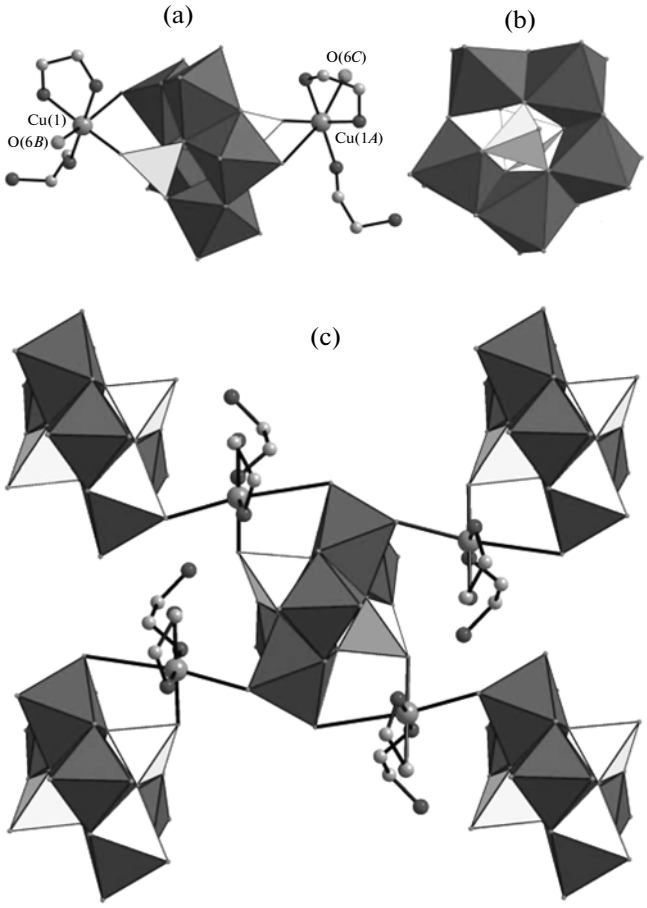

Fig. 1. Polyhedral/ball-and-stick view of the molecular structural unit of **I** with the selected labeling scheme (a), polyhedral view of the Strandberg-type $[P_2Mo_5O_{23}]^{6-}$ subunit (b), and the combination of each $[P_2Mo_5O_{23}]^{6-}$ subunit with adjacent four same subunits by four $[Cu(En)(EnH)]^{3+}$ bridges (c). The atoms with the suffix *A*, *B* and *C* are generated by the symmetry operation: (*A*) $-1-x, 0.5-y, z$; (*B*) $-0.5-x, -0.5+y, z$; (*C*) $-0.5+x, 1-y, z$.

sharing corners which is significantly longer (3.692 Å). The Mo–P distances are in the range 3.348–3.680 Å and the P–P distance is 3.826 Å. These distances are good agreement with the reported values [10]. In the molecular structural unit of **I**, two centrosymmetric $[Cu1(En)(EnH)]^{3+}$ and $[Cu1A(En)(EnH)]^{3+}$ cations are situnated on both sides of the Strandberg-type $[P_2Mo_5O_{23}]^{6-}$ subunit, each of which covalently links to the $[P_2Mo_5O_{23}]^{6-}$ subunit through two oxygen atoms (one from a MoO_6 octahedron and the other from a PO_4 tetrahedron). Both $[Cu1(En)(EnH)]^{3+}$ and $[Cu1A(En)(EnH)]^{3+}$ cations adopts the six-coordinate elongated octahedral geometry, in which three nitrogen atoms from two En ligands (Cu–N 1.993(3)–2.026(3) Å) and one oxygen atom from a PO_4 tetrahedron (Cu–O 1.958(2) Å) build the basal plane and two oxygen atoms from adjacent two $[P_2Mo_5O_{23}]^{6-}$ subunits occupy two axial positions (Cu–O 2.2578(3)–3.096(3) Å). It is worth noting that there are two crystallo-

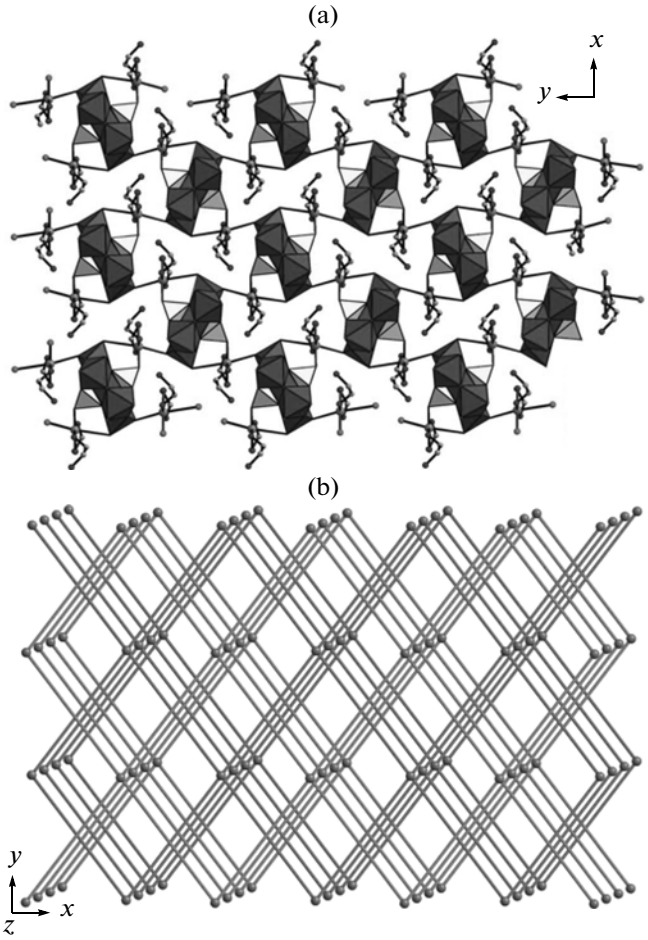

Fig. 2. The 2D sheet architecture of **I** (a) and topological view of the 2D sheets showing the (4,4)-network and the –ABAB– mode (b).

graphically unique En ligands in **I**, which display two different coordination modes in the $[Cu1(En)(EnH)]^{3+}$ cation. One En ligand employs the bidentate chelating mode while the other adopts the monodentate end-on mode. As for organoamines, this monodentate end-on mode is very rare in POM chemistry [29–31]. Obviously, the $[Cu1(En)(EnH)]^{3+}$ coordination cations not only act as countercations that compensate for the anionic charges of the $[P_2Mo_5O_{23}]^{6-}$ subunits, but also act as connectors of the $[P_2Mo_5O_{23}]^{6-}$ subunits, which result in the formation of the 2D sheet structure. Interestingly, the most remarkable feature of **I** is that each molecular structural unit is connected with adjacent four same units by four $[Cu(En)(EnH)]^{3+}$ bridges (Fig. 1c), constructing the 2D organic-inorganic hybrid sheet structure (Fig. 2a). To our knowledge, such 2D hybrid sheet structure constructed from Strandberg-type phosphomolybdate units and copper-organic cation bridges is very rare [14]. From the viewpoint of topology, provided that each molecular structural unit function is viewed as a 4-connected node, the 2D organic-inorganic hybrid sheet structure is the 2D (4,4)-topological net (Fig. 2b). Adjacent 2D (4,4)-topological nets are aligned in the mode of –ABAB– (Fig. 2b). In POM chemistry, similar 2D (4,4)-topological network with the alignment mode of –ABAB– has been observed in an octa-Cu sandwiched germanotungstate $[Cu_2(H_2O)_2(2,2'\text{-Bipy})_2]\{[Cu(Bdyl)]_2[Cu_8(2,2'\text{-Bipy})_4(H_2O)_2(B\text{-}\alpha\text{-}GeW_9O_{34})_2]\} \cdot 4H_2O$ [32]. In addition, 2D (4,4)-topological networks with the alignment mode of –AAA– have been also encountered in $\{[Ni(Dap)_2(H_2O)]_2[Ni(Dap)_2]_2[Ni_4(HDap)_2(\alpha\text{-B-}HSiW_9O_{34})_2]\} \cdot 7H_2O$ [29], $\{[Ni(Dap)_2(H_2O)]_2[Ni(Dap)_2]_2[Ni_4(HDap)_2(\alpha\text{-B-}HGeW_9O_{34})_2]\} \cdot 6H_2O$ [29], $\{[Ni(Dap)_2(H_2O)]_2[Ni(Dap)_2]_2[Ni_4(HDap)_2(\alpha\text{-B-}PW_9O_{34})_2]\} \cdot 4H_2O$ [29], and $[DMAH]_4\{[Mn(DMF)_4]_2[Mn_4(DMF)_2(\alpha\text{-B-}HPW_9O_{34})_2]\}$ [31].

It is well known that the IR spectroscopy is a good method for identifying the structual type of POM polyoxoanions and the presence of organic components. The IR spectrum of **I** exhibits the characteristic vibration pattern derived from the Strandberg-type polyoxoanions in low-wavenumber region. The obvious absorption bands at 1108 and 1044 cm^{-1} are assigned to the $\nu(P{-}O_t)$ and $\nu(P{-}O_b)$ stretching vibrations, respectively [10]. The absorption band at 962 cm^{-1} is attributed to the $\nu(W{-}O_t)$ stretching vibrations while the strong absorption band at 898 cm^{-1} is ascribed to the $\nu(W{-}O_b)$ stretching vibrations [10]. The strong absorption band at 681 cm^{-1} corresponds to the breathing of the $[P_2Mo_5O_{23}]^{6-}$ subunit [10]. These results are well comparable to those recorded in [10, 14]. In comparison with those of $\alpha\text{-}Na_2HPMo_{12}O_{40} \cdot 14H_2O$ (962, 1068, 869, and 785 cm^{-1} for $\nu(W{-}O_t)$, $\nu(P{-}O_a)$, $\nu(W{-}O_b)$, and $\nu(W{-}O_c)$) [16], the $\nu(P{-}O)$ absorption band splits into two absorption peaks due to the existence of two types of stretching mode ($\nu(P{-}O_t)$ and $\nu(P{-}O_b)$) in **I**. The difference of the W–O absorption bands between them mainly result from the distinction of their structural types of POM moieties ($\alpha\text{-}Na_2HPMo_{12}O_{40} \cdot 14H_2O$ belongs to the Keggin-type whereas **I** is the Strandberg-type). The stretching absorption bands of the $-NH_2$ and $-CH_2$ groups are observed at 3233–3150 and 2956–2882 cm^{-1}, and the bending vibration bands of the $-NH_2$ and $-CH_2$ groups also appear 1580 and 1465 cm^{-1} [32]. The presence of these signals confirms the existence of En ligands in **I**. In addition, a broad absorption band at 3444 cm^{-1} must be assigned to the absorption of lattice water molecules. In a word, the results of IR spectrum of **I** are in good agreement with those of single-crystal structural analysis.

The UV spectrum of **I** in the aqueous solution has been performed in the range of 190–400 nm (Fig. 3) and reveals two absorption bands centered at 206 and 229 nm. The higher-energy absorption band is assigned to the $p\pi{-}d\pi$ charge transfer transitions of the $O_t \rightarrow W$ bonds whereas the lower-energy absorption

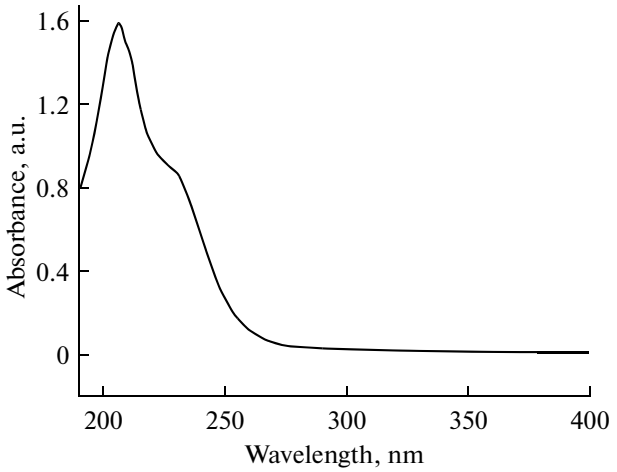

Fig. 3. The UV spectrum of **I** in the aqueous solution.

band is attributed to the $p\pi-d\pi$ charge transfer transitions of the $O_b \rightarrow W$ bonds.

ACKNOWLEDGMENTS

This work was supported by the Natural Science Foundation of China (no. 21101055), China Postdoctoral Science Foundation funded project (nos. 201104392, 20100470996), the Natural Science Foundation of Henan Province (nos. 092300410119, 102300410093), the Postdoctoral Science Foundation of Henan University (no. BH2010003) and the Foundation of Education Department of Henan Province (nos. 2009A150003, 2010B150006).

REFERENCES

1. Reinoso, S. and Galán-Mascarós, J.R., *Inorg. Chem.*, 2010, vol. 49, p. 377.
2. Compain, J.D., Mialane, P., Dolbecq, A., et al., *Angew. Chem. Int. Ed.*, 2009, vol. 48, p. 3077.
3. Wu, Q., Chen, W.L., Liu, D., et al., *Dalton Trans.*, 2011, vol. 40, p. 56.
4. Skibsted, J., Brorson, M., Villadsen, J., et al., *Inorg. Chem.*, 2000, vol. 39, p. 4130.
5. Jin, H.J., Zhou, B.B., Yu, Y., et al., *CrystEngComm*, 2011, vol. 13, p. 585.
6. Cao, R., Liu, S., and Cao, J., *J. Mol. Struct.*, 2008, vol. 888, p. 307.
7. Strandberg, R., *Acta Chem. Scand.*, 1973, vol. 27, p. 1004.
8. Hedman, B., *Acta Chem. Scand.*, 1973, vol. 27, p. 3335.
9. Fisher, J., Ricard, L., and Toledano, P., *Dalton Trans.*, 1974, p. 941.
10. Aranzabe, A., Wéry, A.S.J., Martin, S., et al., *Inorg. Chim. Acta*, 1997, vol. 255, p. 35.
11. Weng, J., Hong, M., Liang, Y., et al., *Dalton Trans.*, 2002, p. 289.
12. Wang, J.P., Wang, Z.L., and Liu, Y.H., *Chin. J. Struct. Chem.*, 2004, vol. 23, p. 695.
13. Upreti, S. and Ramanan, A., *Cryst. Growth Des.*, 2006, vol. 6, p. 2066.
14. Thomas, J. and Ramanan, A., *Cryst. Growth Des.*, 2008, vol. 8, p. 3390.
15. Wang, J.P., Zhao, J.W., Ma, P.T., et al., *Chem. Commun.*, 2009, p. 2362.
16. Rocchiccioli-Deltcheff, C., Fournier, M., Franck, R., et al., *Inorg. Chem.*, 1983, vol. 22, p. 207.
17. Liu, Y., Shi, D.Y., Zhao, J.W., et al., *Inorg. Chem. Commun.*, 2011, vol. 14, p. 1178.
18. Zhang, Z.M., Li, Y.G., Yao, S., et al., *Angew. Chem. Int. Ed.*, 2009, vol. 48, p. 1581.
19. Sheldrick, G.M., *SHELXTL-97, Program for Crystal Structure Solution*, Göttingen (Germany): Univ. of Göttingen, 1997.
20. Brown, I.D. and Altermatt, D., *Acta Cryst.*, *B*, 1985, vol. 41, p. 244.
21. Thorp, H.H., *Inorg. Chem.*, 1992, vol. 31, p. 1585.
22. Hölscher, M., Englert, U., Zibrowius, B., et al., *Angew. Chem., Int. Ed.,* 1995, vol. 33, p. 2491.
23. Pichon, C., Dolbecq, A., Mialane, P., et al., *Chem. Eur. J.*, 2008, vol. 14, p. 3189.
24. Pichon, C., Dolbecq, A., Mialane, P., et al., *Dalton Trans.,* 2008, p. 71.
25. Zhao, J.W., Shi, D.Y., Chen, L.J., et al., *CrystEngComm*, 2011, vol. 13, p. 3462.
26. Bassil, B.S., Nellutla, S., Kortz, U., et al., *Inorg. Chem.*, 2005, vol. 44, p. 2659.
27. Li, B., Zhao, J.W., and Zheng, S.T., *Inorg. Chem.*, 2009, vol. 48, p. 8294.
28. Lowe, M.P., Lockhart, J.C., Clegg, W., et al., *Angew. Chem. Int. Ed.*, 1994, vol. 33, p. 451.
29. Zhao, J.W., Li, B., and Zheng, S.T., et al., *Cryst. Growth Des.*, 2007, vol. 7, p. 2658.
30. Zhang, Z., Liu, J., Wang, E., et al., *Dalton Trans.*, 2008, p. 463.
31. Zhao, J.W., Li, J.L., Ma, P.T., et al., *Inorg. Chem. Commun.*, 2009, vol. 12, p. 450.
32. Zhao, J.W., Wang, C.M., Zhang, J., et al., *Chem. Eur. J.*, 2008, vol. 14, p. 9223.